Nanoscale

Accepted Manuscript

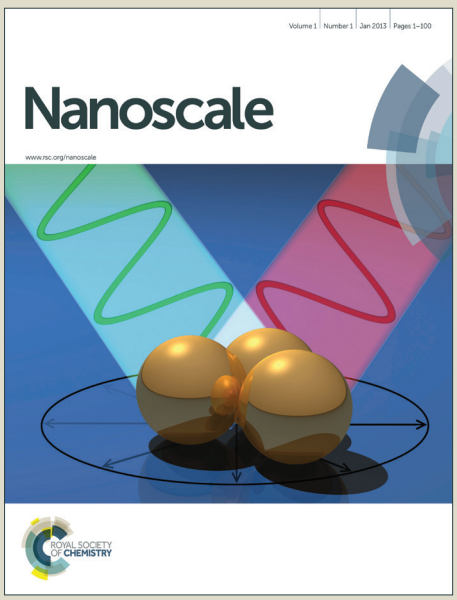

ROYAL SOCIETY OF CHEMISTRY

www.rsc.org/nanoscale

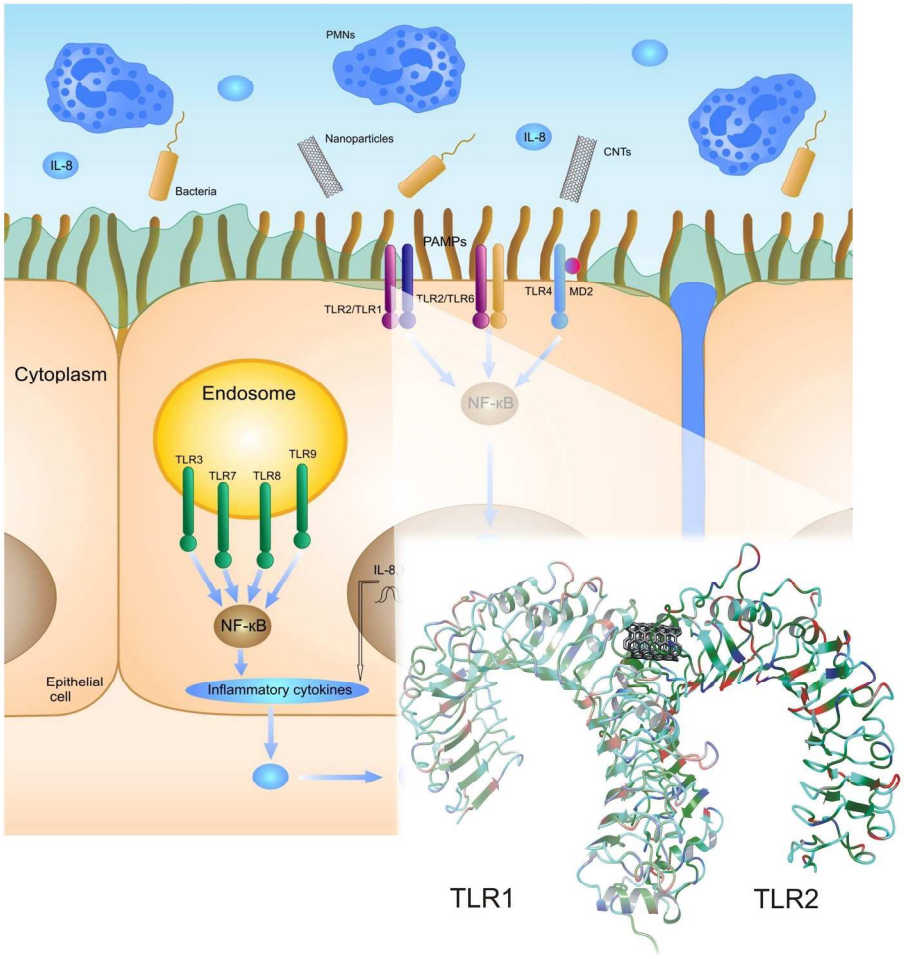

1270x1270mm (61 x 61 DPI)

Immunotoxicity of nanoparticles: Computational study suggests that CNTs and C_{60} fullerenes might be recognized as pathogens by Toll-like receptors

M. Turabekova,[a,b†] *B. Rasulev,*[a†] *M. Theodore,*[c] *J. Jackman,*[c] *D. Leszczynska,*[b] *J. Leszczynski* [a*]

[a]Interdisciplinary Center for Nanotoxicity, Department of Chemistry, Jackson State University, 1400 J. R. Lynch Street, P. O. Box 17910, Jackson, MS 39217, USA

[b]Interdisciplinary Nanotoxicity Center, Department of Civil and Environmental Engineering, Jackson State University, Jackson MS, USA

[c]The Johns Hopkins University, Applied Physics Laboratory, Laurel, MD 20723, USA

[†]These authors contributed equally to this work

ABSTRACT

For the last decade, a big deal of attention is being devoted to study inflammatory response upon exposure to multi/single-walled carbon nanotubes (CNTs) and different fullerene derivatives. In particular, carbon nanoparticles are reported to provoke substantial inflammation in alveolar and bronchial epithelial cells, epidermal keratinocytes, cultured monocyte-

macrophage cells etc. We suggest a hypothetical model providing the potential mechanistic explanation for immune and inflammatory responses observed upon exposure to carbon nanoparticles. Specifically, we performed a theoretical study to analyze CNT and C_{60} fullerene interactions with the available x-ray structures of Toll-like receptors (TLR) homo- and heterodimer extracellular domains. The assumption was based on the fact, that similar to the known TLR ligands both CNT and fullerene induce, in cells, secretion of certain inflammatory protein mediators, such as interleukins and chemokines. These proteins are observed within inflammation downstream processes resulted from ligand molecule dependent inhibition or activation of TLRs –induced signal transduction. Our computational studies have shown that the internal hydrophobic pockets of some TLRs might be capable to bind small-sized carbon nanostructures (5,5 armchair SWCNT containing 11 carbon atom layers and C_{60} fullerene). High binding scores and minor structural alterations induced in TLR ectodomains upon binding C_{60} and CNT further supported our hypothesis. Additionally, the proposed hypothesis is strengthened by the indirect experimental findings indicating that CNTs and fullerene induce an excessive expression of specific cytokines and chemokines (i.e. IL-8 and MCP1).

Keywords: Nanoparticles, Toll-like receptors, immunotoxicity, interleukines, molecular docking

Introduction

Understanding toxicology of nanoparticles requires contributions from various disciplines. Toxicological risk assessment of occupational exposures to manufactured carbon nanotubes (CNTs) has been reviewed by Lam *et al.*[1], while application of computational methods for such assessments have been discussed in our recent publication[2]. Previously we demonstrated that computational approaches are able to predict properties of nanoparticles[2-6] and toxicity of nano metal oxides[7]. Various studies indicate a strong impact of carbon nanostructures on the immune system,[8-13] by inducing pro-inflammatory activity.[14-16] Pattern recognition receptors (PRRs) represent a primitive part of the immune system and are known to play a crucial role in the detection of invading pathogens and subsequent activation of the innate immune response.[17,18] This response provides the first line of defense against infectious disease or other alien substances. Transmembrane proteins such as Toll-like receptors (TLRs),[19,20] belong to

membrane-bound PRRs type and recognize specific and conserved pathogen-associated molecular patterns (PAMPs) present in microbial proteins, nucleic acids, lipids, and carbohydrates. These PAMP-containing molecules act as ligands to trigger PRR-dependent intracellular signaling pathways that ultimately induce the expression of pro-inflammatory and antiviral cytokines. Secretion of these cytokines at the site of an infection promotes the recruitment of neutrophils and natural killer (NK) cells, which eliminate pathogenic objects and infected cells. Therefore, TLRs act as the forefront PAMPs' recognizers in the cells involved with the immune system (e.g. macrophages).[21,22] Each TLR is responsible for the particular set of PAMPs.

Scheme 1.

TLRs play crucial role in triggering innate immune responses as they recognize pathogen-derived molecules.[17,18,23,24] Although, each TLR is characterized by distinct ligand-binding area, they all form "m"-shaped homo- or heterodimers, thereby supporting hypothesis of such dimerization invoking subsequent activation of intracellular Toll/Interleukin-1 receptor (TIR) domains [17, 24]. While a few crystallographic structures of TLR extracellular domains (ECDs) with bound antagonist/agonist molecules have been reported,[24-28] no further information on target interaction sites is available for the remaining large group of compounds, including carbon nanostructures. For the last decade, a lot of attention is being devoted to study inflammatory response upon exposure to multi/single-walled CNTs and different fullerene derivatives. Particularly, the exposure to these carbon nanoparticles inevitably provokes substantial

inflammation in alveolar and bronchial epithelial cells, epidermal keratinocytes, cultured monocyte-macrophage cells etc.[29-34]

The recent studies on CNTs inflammatory effect showed extremely interesting findings. Thus, CNTs are reported to promote IL-1ß and IL-18 secretion in the presence of TLR ligands (LPS, peptidoglycan, PAM_3SCK_4 etc).[35] Also, when highly purified, these nanoparticles failed to stimulate any detectable level of inflammatory cytokine secretion.[36] According to the so-called bio-corona concept nanoparticles may selectively absorb biomolecules including LPS, bacterial endotoxin, phospholipid etc. when exposed to physiological environment.[37, 38] These molecules are membrane components of bacteria or apoptotic cells and known to serve as an "eat-me" signal for macrophages.[37, 38] Although no further information is available on the detailed mechanism, one cannot rule out the possibility of coated CNTs being brought directly at the site of action of coating molecules. This may serve as an additional factor promoting CNT-TLR interactions considered in this paper. Moreover, to access a TLR's active site lengthy CNTs should be reduced into the small fragments. Interestingly, there is a recent evidence on the existence of human enzyme "myeloperoxidase" (hMPO) participating in biodegradation of carbon nanotubes by breaking them down to the smaller pieces.[39] This finding actually strongly supports hypothesis proposed below, since smaller pieces of CNTs can easily interact with TLRs.

In this study we present a hypothesis of CNT-TLR and C_{60}-TLR interaction mechanism, as one of the possible mechanisms of inflammation response when cells are exposed to carbon nanostructures. We performed a computational modeling to investigate the 5,5 armchair SWCNT of 11-carbon atom layers, and C_{60} fullerene interactions with the species representing available x-ray structures of TLR homo- and heterodimer extracellular domains, such as TLR1/TLR2 [25],

TLR2/TLR6 [27], TLR2 [27], TLR4 [22], TLR5 [28], and TLR3 [40]. The assumption was based on aforementioned indirect evidences[35, 36, 37, 38] and the fact, that similarly to the known TLR ligands (LPS, Pam_3CSKA_4, Eritoran etc), CNT and fullerene induce in cells secretion of certain inflammatory protein mediators, such as interleukins and chemokines. These proteins are observed within inflammation downstream processes resulted from ligand molecule dependent inhibition or activation of TLRs –induced signal transduction. Given that structural experimental details are yet to be discovered for the carbon nanomaterial-TLR interaction, the binding sites of the existing agonist/antagonist TLR ligands were explored at the first instance. Here, we also report experimental data of CNTs and C_{60} on cytokine assays (Supplementary Information, Table S1 and Figure S1). Based on computational studies coupled with the discussed experimental findings we propose the mechanistic model describing interactions between considered carbon nanoparticles Toll-like receptor proteins.

Methods

Computational Methods

SiteMap and Docking calculations

The crystal structures of the following TLR external domains were obtained from RCSB Protein Data Bank: TLR1/TLR2 (2Z7X), TLR2/TLR6 (3A79), TLR2 (3A7C, 3A7B), TLR4/MD (3FXI), TLR5 (3V47), TLR3 (2A0Z). Next, the "Protein Preparation Wizard" (Schrödinger Suite 2011 Protein Preparation Wizard) workflow in Maestro 9.2 (Maestro, version 9.2, Schrödinger, LLC, New York, NY, 2011[41]) was applied. This included removal of crystallographic water molecules and co-crystalized ligand molecules, addition of hydrogen atoms followed by

assignment of bond orders, partial charges (based on OPLS-2005 force field) and protonation states. Next, the orientations of hydroxyl groups, amide groups of Asn and Gln and charge state of His residues were optimized. All final His residues were assigned as neutral. Finally, the Impact Refinement module (Impref) was applied to minimize protein structure using OPLS-2005 force field. Minimization was terminated upon a root-mean-square deviation of all heavy atoms reached cutoff of 0.3 Å resulting in removal of steric clashes and bad contacts.

SiteMap 2.5 (SiteMap, version 2.5, Schrödinger, LLC, New York, NY, 2011[41]) was applied for the binding sites prediction. A one-angstrom grid of possible site points was placed around the entire protein. Next, the site points were classified into "inside" or "outside" points based on the comparison of the distance to the nearby protein atoms to the van der Waals radius of those atoms. The point was considered as "outside" given the ratio of the squares of these distances was larger than 2.5 Å. The "outside" points were additionally examined for the subject of good van der Waals contact with the receptor (at the least distance of 4 Å) and being sufficiently enclosed by it (the fraction of rays striking the receptor surface at a distance 8 Å has to be larger than 0.5). The site points groups with minimum of 3 candidate site points at the maximum squared distance of 3.1 Å were kept. Further, all eligible site point groups with minimum required size of 15 site points within 6.5 Å were merged and 5 best sites kept for the following generation of contour maps. In particular, for the each returned site the five maps, including hydrophobic, hydrophilic (further divided into donor and acceptor) and surface were constructed using the default settings. Finally, the site point groups together with produced grid maps were evaluated in terms of a number of calculated properties. The computed properties include:

Number of Site Points – typically 2 to 3 site points are found for each atom of the bound ligand. The bigger size is an indicator of a preferable binding site.

SiteScore – a weighted sum of several properties. For a promising binding site this score is above 1.0.

Druggability Score – is a similar parameter to SiteScore, though uses different coefficients. This option is designed to distinguish those molecules binding tightly but not of drug-like nature.

Site Volume is calculated ensuring the protein site is well enclosed by the protein.

Receptor Grid Generation tool within Glide docking program (Glide, version 5.7, Schrödinger, LLC, New York, NY, 2011[41]) was applied to generate grid box with the average dimensions for CNT 24 Å x 24 Å x 24 Å (outer) and 14 Å x 14 Å x 14 Å (inner), and fullerene 14 Å x 14 Å x 14 Å (outer) and 10 Å x 10 Å x 10 Å (inner).

The Glide rigid docking runs were performed with the extra-precision mode (XP) mode. The scaling of van der Waals radii for ligand's non-polar atoms was set to 0.8 with up to 3 best poses per ligand saved. No constraints were applied for considered carbon nanostructures.

Experimental Methods

Fullerene-C_{60} and CNTs (double-walled CNTs - 900-1500-1G-) were obtained from SES Research (Houston, TX) and used as is for the present study. Detailed procedure for the solubilization of the fullerene-C_{60} and nanotubes is reported elsewhere. Human lung carcinoma epithelial cell line (A549) was used in experiments. The activation by CNTs of the NF-κB signaling pathway in macrophages by increasing the secretion of a panel of cytokines and chemokines that promote inflammation is measured (see Supplementary Information, Table S1 and Figure S1).

Results and Discussion

The computational study was initiated by analyzing binding sites on and within TLRs ectodomains in order to identify the sites potentially suitable for the interactions with carbon nanotube and fullerene C_{60}. The selected binding sites had to be primarily hydrophobic in nature and of the size capable to fit studied CNT and C_{60} fullerenes.

Identification of hydrophobic binding sites

The SiteMap[41,42] analysis run for a series of TLR external domains yielded a number of interesting observations. The parameters calculated for the best scored site of the each TLR ECD are collected in Table 1. Out of 5 sites produced by SiteMap, one site with the highest number of site points (parameter "size") was kept for further discussion. First, the sites containing prevalent hydrophobic over hydrophilic areas were identified as the highest scored sites for the majority of TLRs, except TLR3 and TLR5. The "*balance"* parameter, which is the ratio of hydrophobic and hydrophilic characters of a molecule, showed to be well above the average value (1.6), due to the predominant contribution of hydrophobicity: 2.080 (TLR2), 4.018 (TLR1/TLR2), 5.049 (TLR2/TLR6) and 62.304 for TLR4/MD. Second, the location of hydrophobic regions were correctly identified for the TLR ECDs (TLR1/TLR2, TLR2/TLR6, TLR2) and MD-2 pocket (TLR4/MD), that are known to bind lipophilic ligand molecules. Thus, a long hydrophobic channel harbored within convex side of TLR1/TLR2 (Fig. 1 a, b), TLR2/TLR6 (Fig. 1 c, d) ECDs, and an inner hydrophobic area within TLR2 ECD (Fig.1 g) and MD-2 (Fig. 1 e, f) are identified as the top-scoring sites. As expected, similarly to TLR4 and TLR5 ECDs, no hydrophobic area was found within TLR3 ECD, suggesting hydrophilic nature of interactions inherent in this particular TLR. Further evaluation of the top-ranked site volumes with large internal hydrophobic regions revealed, that they are capable to accommodate fullerene and CNTs

of certain sizes. This led us to hypothesize that TLRs might also participate in hydrophobic interactions with nanomaterials or modify standard ligand responses.

Figure 1.

Table 1.

Nanostructure-TLR docking

Molecular docking of C_{60} and 5,5 armchair SWCNT into TLR1/TLR2, TLR2/TLR6, TLR2 ECDs and TLR4 MD-2 pocket were carried out in order to evaluate the binding affinity of studied nanomaterials towards TLR ECDs. For this, C_{60} fullerene and 5,5 SWCNT were placed arbitrarily within TLR ECDs internal hydrophobic areas followed by Impref OPLS-2005 force field minimization of the obtained TLR-nanomaterial structures. The Glide XP binding score values obtained for the C_{60} and 5,5 SWCNT are collected in Table 2. The data clearly indicated that the selected docking regions were well-suited for the studied carbon nanostructures. Thus, a strong interaction energy, which mainly consisted of the van der Waals term, was observed between the nanoparticle cage and a protein. Generally, the higher binding scores were obtained for the nanotube-TLR binding than for fullerene-TLR, owing to tube's larger surface area. In most cases, the 5,5 CNT GScore together with Glide energy values were up to as twice as higher than those for C_{60}. In fact, our computational data is in line with recently published computational reports on the importance of nanoparticle hydrophobicity in binding with some proteins[43,44] and also experimental report on hydrophobicity importance for immune system activation[45]. Namely, a strong linear correlation was established between a size of hydrophobic coating for gold nanoparticles and mRNA expression associated with a number of cytokines.

Functional groups of higher hydrophobicity nature (logP) were found to induce relatively higher immune response.[45] As we discussed above the use of small sized CNTs in our simulations is justified by the recent evidence on the existence of human enzyme "myeloperoxidase", hMPO, participating in biodegradation of carbon nanotubes by breaking them down into the smaller pieces.[39] This evidence supports our hypothesis, since "minced" pieces of CNTs can easily interact with TLRs.

Next, we generated interaction diagrams for the highest scored poses of nanotube and fullerene with the considered hydrophobic receptor sites. The amino acid residues located within 4Å radius from bound nanostructures are collected in Table S3. As can be seen from the Figure 2a-b, CNT and C_{60} are surrounded by amino acids of mostly hydrophobic nature giving rise to strong van der Waals interactions. A close examination of the receptor site revealed the details on the origin of the observed vdW forces. In particular, numerous Phe and Tyr residues could easily form π-π interactions, while an excessive number of the rest hydrophobic amino acids (Leu, Ile, Ala, Val, Pro) favored lipophilic contacts with the sidewalls of CNT and fullerene. This observation is consistent with TLR interactions with its natural ligands, lipopolysaccharides. Also, a couple of positively charged lysines were found to be capable of forming π-cation bonding. For TLR5, docking of nanostructures into the identified hydrophobic receptor site produced π-π interactions with phenylalanines from both ectodomains (Phe273 and Phe371) with an additional π-cation interaction with both ECDs Arg377.

Table 2.

Figure 2.

Table 3.

Unlike other LRR family proteins, the central domains of TLRs 1, 2, 4 and 6 have irregular LRR sequences and a lack of stabilizing asparagine networks. This results in bumpy convex surfaces of TLRs suitable for interactions with non-protein ligands and also in allowed partial distortions of the central part.[17, 24] In the Figure 2(b), we have aligned the structure of TLR2 ECDs before (green carbon atoms) and after (blue carbon atoms) OPLS2005 refinement upon binding of CNT. The carbon nanotube is placed within TLR1/TLR2 hydrophobic channel, so that the greater part of CNT interacts with TLR2 and a smaller with TLR1 ectodomains. It can be seen from the Figure 2(b) that two parallel loops form the entrance to the binding pocket and are aligned by hydrophobic acids. In crystallographic structure of TLR2 ECD, the side chains of Phe349, Phe325 and Leu328 seem to impede carbon nanotube from moving further towards the inner part of the hydrophobic pocket. However, owing to the allowed flexibility of the central domain loops, the orientation of the mentioned amino acid side chains can easily be altered, leaving the binding pocket open for nanostructures (fullerene and CNT). Next, CNT was also shown to form van der Waals contacts with interfacial amino acids at the edge of hydrophobic pocket on TLR1 ECD. Moreover, the size of inner pocket was sufficient to accommodate a larger portion of a nanotube, provided the orientation of Phe312, Phe314, Trp258 and Gln316 side chains were optimized accordingly. Fullerene exhibited higher affinity to the TLR2 ECD inner hydrophobic pocket (GScore = -12.88 kcal/mol) than to the TLR1/TLR2 dimer interface. Unlike fullerene, 5,5 CNT showed equally good binding towards TLR1/TLR2 (-15.4 kcal/mol) and TLR2/TLR6 (-20.0 kcal/mol) heterodimerization interface areas and TLR2 internal pocket (-2.7 kcal/mol). Interestingly, as indicated by SiteMap results (Table 1), a substantial increase of the binding site volume (from 637.98 to 1536Å^3) and its size (from 355 to 423 site points) was

observed for the Impact refined structure of CNT-bound TLR2/TLR6 structure. This can be explained by the structural peculiarities of LRR proteins that form solenoid structure, in which hydrophobic residues point to the interior. A lipophilic ligand intrusion into the hydrophobic TLR6 ECD will result in subsequent re-orientation of the consensus hydrophobic side chains allowing more space for the ligand accommodation.

MD-2 is a co-receptor molecule that binds to TLR4 ECD by mediating mostly hydrophilic and a few hydrophobic interactions.[46] MD2 belongs to β-cup lipid-binding proteins family with antiparallel β sheets and conserved disulfide bridges. The inner side of MD-2 represents a deep and narrow hydrophobic pocket, which opening is lined with positively charged residues. Unlike other globular proteins, MD-2 lacks sizable hydrophobic core and therefore is known to bind large and structurally different ligands.[17, 24] The docking calculations of MD-2 with C_{60} and 5,5 CNT revealed that co-receptor's internal hydrophobic pocket can accommodate both carbon nanostructures (Fig.3a,b): the binding scores are -9.3 kcal/mol and -16.7 kcal/mol for fullerene and CNT, correspondingly. The alignment of both co-receptors before and after OPLS2005 refinement showed that little change is induced in overall structure of MD-2 upon carbon nanostructures binding. The only visible re-orientation occurred for the side chains of Phe121, Glu92 at the pocket entrance and Phe76, Leu78, Phe147 and Leu61 inside of the pocket. This also supports the fact of MD-2 internal hydrophobic pocket being large enough to accommodate ligands of bigger size.

Figure 3.

In summary, our computational studies have shown that the internal hydrophobic pockets of TLR1/TLR2, TLR2/TLR6 ECDs and MD-2 might be capable to bind two types of carbon nanostructures - 5,5 armchair SWCNT of 11-carbon atom layers and C_{60} fullerene. High binding scores and minor structural alterations induced in TLR ECDs upon binding C_{60} and CNT further supported our hypothesis. The applied SiteMap search engine was able to locate hydrophobic regions followed by their size and shape examination. Although our computational models are yet to be confirmed experimentally, the possibility of carbon nanostructures interacting with the hydrophobic pockets on TLR ECDs cannot be ruled out. In part, our hypothesis is supported by the indirect finding that CNTs and fullerene induce excessive expression of specific cytokines and chemokines (e.g. IL-8 and MCP-1).

The prediction of binding sites and candidate ligands is not straightforward for cells undergoing multistep TLRs induced inflammation processes. Therefore, more future structural and biochemical studies are needed to shed light on the type of interactions for the involved carbon nanoparticles. Until then, computational studies come very handy and we believe our results might aid in further carbon nanostructures toxicity prediction.

Author Information

Corresponding Author

*Email: jerzy@icnanotox.org; Telephone: +1 (601) 979-3482; Fax: +1 (601) 979-6865

Notes

The authors declare no competing financial interest.

Acknowledgements

The authors would like to thank for support from the Johns-Hopkins University (Laurel, Maryland) for the funding grant No. 956126 “Theoretical Modeling of Nanotoxicity”, National Science Foundation for the DMR-0611539 PREM grant; and for the NSF EPSCoR Grant No. 362492-190200-01\NSFEPS-0903787. Authors also thank the Extreme Science and Engineering Discovery Environment (XSEDE) for award allocation number TG-DMR110088 and Mississippi Center for Supercomputer Research (Oxford, MS) for a generous allotment of a computer time.

Abbreviations

TLR, Toll-like receptor; ECD, extracellular domain; CNT, Carbon nanotube; SWCNT, Single walled carbon nanotube; MD-2, Myeloid differentiation factor-2; LPS, Lipopolysaccharide

References

1. C. W. Lam, J. T. James, R. McCluskey, S. Arepalli and R. L. Hunter, *Critical Rev. Toxicol.*, 2006, 36, 189-217.
2. A. Gajewicz, B. Rasulev, T. C. Dinadayalane, P. Urbaszek, T. Puzyn, D. Leszczynska, J. Leszczynski, *Adv. Drug Del. Rev.*, 2012, 64, 1663-1693.
3. Leszczynski. *Nat. Nanotech.,* 2010, 5, 633–634.
4. L. Ahmed, B. Rasulev, M. Turabekova, D. Leszczynska, J. Leszczynski, *Org. Biomol. Chem.*, 2013, 11, 5798-5808J.
5. T. Puzyn, D. Leszczynska, J. Leszczynski, *Small,* 2009, 5, 2494-2509.
6. (a) T. Petrova, B. Rasulev, A. A. Toropov, D. Leszczynska, J. Leszczynski, *J. Nanopart. Res.*, 2011, 13, 3235-3247; (b) A. A. Toropov, B. Rasulev, D. Leszczynska, J. Leszczynski, *Chem. Phys. Lett.,* 2008, 457, 332-336; (c) A. A. Toropov, B. Rasulev, D. Leszczynska, J. Leszczynski, *Chem. Phys. Lett.*, 2007, 444, 209-214; (d) A. Furmanchuk, O. Isayev, T. C. Dinadayalane, D. Leszczynska, J. Leszczynski, *WIREs Comput. Mol. Sci*, 2012, 2, 817-828; (e) T. C. Dinadayalane, J. Leszczynski, In *Handbook of Computational Chemistry*, Springer, Heidelberg, 2012, 2, pp. 793–867; (f) B. Rasulev, A. Gajewicz, T. Puzyn, D. Leszczynska, J. Leszczynski, In *Towards Efficient Designing of Safe Nanomaterials*, ed. J. Leszczynski, T. Puzyn, *RSC Nanosci. Nanotech.*, 2012, ch. 10, pp. 220-256; (g) T. C. Dinadayalane, D.

Leszczynska, J. Leszczynski, S. Saha, *Chem. Phys. Lett.*, 2012, 541, 85–91; (h) B. Rasulev, D. Leszczynska, J. Leszczynski, In *Advanced Methods and Applications in Chemoinformatics: Research Progress and New Applications*, 2011, ch. 3, 92-110.
7. (a) T. Puzyn, B. Rasulev, A. Gajewicz, X. Hu, T. P. Dasari, A. Michalkova, H. –M. Hwang, A. Toropov, D. Leszczynska, J. Leszczynski, *Nat. Nanotech.,* 2011, 6, 175-178; (b) A. Gajewicz, T. Puzyn, B. Rasulev, D. Leszczynska, J. Leszczynski, *Nanosci. Nanotech. – Asia*, 2011, 1, 53-58; (c) A. A. Toropov, A. P. Toropova, E. Benfenati, G. Gini, T. Puzyn , D. Leszczynska, J. Leszczynski, *Chemosphere*, 2012, 89, 1098–1102.
8. C. Chang, *J. Autoimmun.*, 2010, 34, J234-J246.
9. K. I. Inoue, *Environ. Health Prevent. Med.*, 2011, 16, 139-143.
10. J. Meng, M. Yang, F. Jia, Z. Xu, H. Kong and H. Xu, *Nanotoxicology*, 2011, 5, 583-591.
11. E. Witasp, A. A. Shvedova, V. E. Kagan and B. Fadeel, *Inhalation Toxicol.*, 2009, 21, 131-136.
12. T. A. M. Uo, F. Watari, Y. Sato, K. Tohji, *Dent. Mater. J.* , 2011, 30, 245-263.
13. L. A. Mitchell, J. Gao, R. V. Wal, A. Gigliotti, S. W. Burchiel and J. D. McDonald, *Toxicol. Sci.*, 2007, 100, 203-214.
14. K. Aschberger, H. J. Johnston, V. Stone, R. J. Aitken, S. M. Hankin, S. A. K. Peters, C. L. Tran and F. M. Christensen, *Crit. Rev. Toxicol.*, 2010, 40, 759-790.
15. M. Davoren, E. Herzog, A. Casey, B. Cottineau, G. Chambers, H. J. Byrne and F. M. Lyng, *Toxicol. In Vitro*, 2007, 21, 438-448.
16. C. W. Lam, J. T. James, R. McCluskey and R. L. Hunter, *Toxicol. Sci.*, 2004, 77, 126-134.
17. I. Botos, D. M. Segal and D. R. Davies, *Structure*, 2011, 19, 447-459.
18. L. A. J. O'Neill, C. E. Bryant and S. L. Doyle, *Pharmacol. Rev.*, 2009, 61, 177-197.
19. S. Akira and K. Takeda, *Nature Reviews Immunology*, 2004, 4, 499-511.
20. K. Takeda, T. Kaisho and S. Akira, Toll-like receptors, 2003, vol. 21, pp. 335-376.
21. S. Akira, S. Uematsu and O. Takeuchi, *Cell*, 2006, 124, 783-801.
22. H. Hemmi, O. Takeuchi, T. Kawai, T. Kaisho, S. Sato, H. Sanjo, M. Matsumoto, K. Hoshino, H. Wagner, K. Takeda and S. Akira, *Nature*, 2000, 408, 740-745.
23. S. Basith, B. Manavalan, R. G. Govindaraj and S. Choi, *PLOS One*, 2011, 6, e23989.
24. J. Y. Kang and J.-O. Lee, *Annu. Rev. Biochem*, 2011, 80, 917-941.
25. M. S. Jin, S. E. Kim, J. Y. Heo, M. E. Lee, H. M. Kim, S.-G. Paik, H. Lee and J.-O. Lee, *Cell*, 2007, 130, 1071-1082.
26. M. S. Jin and J.-O. Lee, *Curr. Opin. Immunol.*, 2008, 20, 414-419.
27. J. Y. Kang, X. Nan, M. S. Jin, S.-J. Youn, Y. H. Ryu, S. Mah, S. H. Han, H. Lee, S.-G. Paik and J.-O. Lee, *Immunity*, 2009, 31, 873-884.
28. S. Yoon, O. Kurnasov, V. Natarajan, M. Hong, A. V. Gudkov, A. L. Osterman and I. A. Wilson, *Science*, 2012, 335, 859-864.
29. R. Baktur, H. Patel and S. Kwon, *Toxicol. In Vitro*, 2011, 25, 1153-1160.
30. D. Crouzier, S. Follot, E. Gentilhomme, E. Flahaut, R. Arnaud, V. Dabouis, C. Castellarin and J. C. Debouzy, *Toxicol. Appl. Pharmacol.*, 2010, 272, 39-45.
31. E. Herzog, H. J. Byrne, A. Casey, M. Davoren, A.-G. Lenz, K. L. Maier, A. Duschl and G. J. Oostingh, *Toxicol. Appl. Pharmacol.*, 2009, 234, 378-390.
32. E.-J. Park, H. M. Kim, Y. Kim, J. Yi, K. Choi and K. Park, *Toxicol. Appl. Pharmacol.*, 210, 244, 226-233.
33. C. Qu, L. Wang, J. He, J. Tan, W. Liu, S. Zhang, C. Zhang, Z. Wang, S. Jiao, S. Liu and G. Jiang, *Gene*, 2012, 493, 9-12.

34. J. G. Rouse, J. Yang, A. R. Barron and N. A. Monteiro-Riviere, *Toxicol. In Vitro*, 2006, 20, 1313-1320.
35. E. Meunier, A. Coste, D. Olagnier, H. Authier, L. Lefèvre, C. Dardenne, J. Bernad, M. Béraud, E. Flahaut and B. Pipy, *Nanomedicine: Nanotechnology, Biology, and Medicine*, 2012, 8, 987–995.
36. M. Yang, K. Flavin, I. Kopf, G. Radics, C. H. A. Hearnden, G. J. McManus, B. Moran, A. Villalta-Cerdas, L. A. Echegoyen, S. Giordani and E. C. Lavelle, *Small*, 2013. DOI:10.1002/smll.201300481
37. B. Fadeel, *Swiss Med Wkly*, 2012, 142, w13609.
38. K. Bhattacharya, F. T. Andón, R. El-Sayed and B. Fadeel, *Adv. Drug Del. Rev.,* 2013, 65, 2087–2097
39. V. E. Kagan, N. V. Konduru, W. Feng, B. L. Allen, J. Conroy, Y. Volkov, I. I. Vlasova, N. A. Belikova, N. Yanamala, A. Kapralov, Y. Y. Tyurina, J. Shi, E. R. Kisin, A. R. Murray, J. Franks, D. Stolz, P. Gou, J. Klein-Seetharaman, B. Fadeel, A. Star and A. A. Shvedova, *Nature Nanotechnology*, 2010, 5, 354-359.
40. J. K. Bell, I. Botos, P. R. Hall, J. Askins, J. Shiloach, D. M. Segal and D. R. Davies, *Proc. Natl. Acad. Sci.,* 2005, 102, 10976-10980.
41. Schrodinger Suite, Schrödinger, LLC, New York, NY, 2011.
42. T. A. Halgren, *J. Chem. Inf. Model.*, 2009, 49, 377-389.
43. M. Calvaresi and F. Zerbetto, *Nanoscale*, 2011, 3, 2873-2881.
44. M. Calvaresi and F. Zerbetto, *ACS Nano*, 2010, 4, 2283-2299.
45. D. F. Moyano, M. Goldsmith, D. J. Solfiell, D. Landesman-Milo, O. R. Miranda, D. Peer and V. M. Rotello, *J. Am. Chem. Soc.*, 2012, 134, 3965-3967.
46. B. S. Park, D. H. Song, H. M. Kim, B.-S. Choi, H. Lee and J.-O. Lee, *Nature*, 2009, 458, 1191-1195.

Table 1. Sitemap calculated the best scored surfaces data.

ECD TLR	Site Score	Size	Dscore	Volume	Exposure	Enclosure	contact	Hydrophobic	Hydrophilic	Balance	Donor/ Acceptor
TLR1/TLR2	1.178	593	1.246	1035.86	0.343	0.839	1.126	2.435	0.606	4.018	0.860
TLR2/TLR6	1.175	355	1.249	637.98	0.344	0.821	1.080	2.840	0.562	5.049	1.132
TLR2/TLR6[1]	1.133	423	1.192	1536.64	0.558	0.798	0.921	1.645	0.697	2.361	0.936
TLR2	1.079	385	1.125	1182.66	0.481	0.750	1.002	1.690	0.813	2.080	1.435
TLR3	0.814	69	0.815	215.06	0.727	0.587	0.802	0.212	0.976	0.217	0.629
TLR4/MD	1.274	152	1.417	596.82	0.575	0.825	0.867	3.413	0.055	62.304	0.782
TLR5	0.983	133	1.034	417.43	0.763	0.617	0.794	0.559	0.847	0.661	0.654

[1] Impact and Glide XP refined CNT-bound structure

Table 2. Glide XP docking scores for the best orientations of fullerene and CNT within hydrophobic areas of TLR ECDs

	Glide GScore	Glide VDW	Glide Emodel	Glide Energy
TLR2 (inside of the convex part)				
C60 fullerene	-12.880	-54.751	-97.882	-54.751
CNT	-22.704	-103.716	-254.823	-102.456
TLR1/TLR2(dimerization interface)				
C60 fullerene	-8.747	-57.345	-87.556	-57.345
CNT	-15.460	-97.621	-234.274	-96.377
MD-2 pocket (TLR4/MD-2)				
C60 fullerene	-9.290	-46.469	-77.114	-46.469
CNT	-16.663	-64.989	-27.314	-64.757
TLR2/TLR6 (dimerization interface)				
C60 fullerene	-9.772	-61.697	-116.919	-61.697
CNT	-20.039	-107.829	-228.650	-108.344
TLR5/TLR5(dimerization interface)				
C60 fullerene	-6.767	-44.897	-77.755	-44.897
CNT	-12.965	-89.693	-218.236	-89.694

Table S3. Amino acid residues within 4Å from C_{60} and 5,5 CNT docked into the TLR1/TLR2, TLR2 TLR2/TLR6, TLR4/MD-2, homodimer TLR5 ECD hydrophobic pockets

CNT	C60
TLR2	
Pro352[1], Leu355, Leu359, Thr335[2], Leu334, Pro306, Val 309, Leu282, Leu312, Leu273, Phe284, Val269, Leu266, Phe267, Phe295, Met270, Ile304, Leu331, Leu328, Tyr326, Ser346, Phe325, Ile319, Leu289, Val348, Leu317, Ile314, Val343, Ile341, Leu367, Trp386, Val351, Asp327	Phe295, Leu328, Leu331, Thr335, Leu355, Leu359, Val351, Leu312, Val343, Ile341, Val348, Ile314, Ser346, Leu317, Ile319, Phe325, Leu289
TLR1/TLR2	
TLR1 Tyr320, Gln316, Val339, Met338, Arg337[3], Val311, Asp310, Phe312, Gly313, Phe314, Pro315	*TLR2* Phe325, Asp327, Pro352, Leu328, Val351, Leu350, Leu355, Val348, Lys347, Val343, Ser346, Ile319, Tyr326, Phe322, Leu324, Tyr323, Tyr320, Phe349
TLR1 Val311, Phe312, Phe314, Pro315, Gln316	*TLR2* Leu324, Phe325, Tyr323, Val339, Phe349, Leu30
TLR4/MD-2	
Leu78, Val135, Leu149, Phe147, Ile46, Leu61, Ile63, Ile117, Phe104, Ile94, Leu74, Ala137, Phe76, Glu92[4], Phe121, Phe119, Ser57, Phe151, Ile52, Leu54, Ile153, Ile80, Cys133	Leu78, Cys133, Val135, Phe151, Ile32, Leu61, Ile52, Phe119, Phe121, Ile153
TLR2/TLR6	
TLR2 Tyr323, Tyr326, Leu328, Phe325, Ile319, Phe322, Ser346, Lys347, Phe349, Val348, Val351, Phe355, Pro352, Asp327, Tyr376	*TLR6* Leu318, Leu350, Phe317, Phe319, Ile292, Val316, Asn314, Pro342, Tyr325, Phe343, Lys321, Ile344, Leu324, Ala323, Ser320
TLR2 Leu350, Tyr3760	*TLR6* Asn314, Val316, Pro342, Leu324, Phe343, Tyr325, Ile344, Ile292, Lys321, Ser320, Phe319, Leu318, Phe317,
TLR5 homodimer	
Phe273, Phe351, Asn329, Glu327, Arg377, Gly353[5], His375	Phe273, Phe351, Asn329, Glu327, Arg377, Gly353, His375
His375, Asn329, Phe273, Phe351	His375, Asn329, Phe273, Phe351

[1] Hydrophobic [2] Polar [3] Charged positive [4] Charged negative [5] Glycine

Figure Legends

Scheme 1. Schematical representation of Toll-like receptors signaling pathway.

Figure 1. Front and top views of the Sitemap calculated hydrophobic areas (solid yellow surfaces) for TLR1/TLR2 (a,b), TLR2/TLR6 (c,d), TLR4/MD-2 (e,f), TLR2 (g) and TLR5 heterodimer (h).

Figure 2. 5,5 CNT-bound TLR1/TLR2 ECDs: **a.** 5,5 CNT is bound to the TLR1 and TLR2 ECDs interface dimerization area; **b.** Aligned structures of TLR2 ECDs before (green carbon atoms) and after (blue carbon atoms) Impact OPLS2005 refinement upon binding 5,5 CNT. The orientation of two parallel entrance loops and the side chains of hydrophobic Phe349, Phe325 and Leu328 preventing nanotube from intrusion are shown to be optimized.

Figure 3. Nanostructures bound TLR4/MD-2 ECD: a. C_{60} is shown to bind inner MD-2 hydrophobic pocket in TLR4/MD-2; Fullerene and carbon nanotube are both well-accommodated in the MD-2 with induced minimal distortion of the entrance residues.

Scheme 1. Schematical representation of Toll-like receptors signaling pathway.

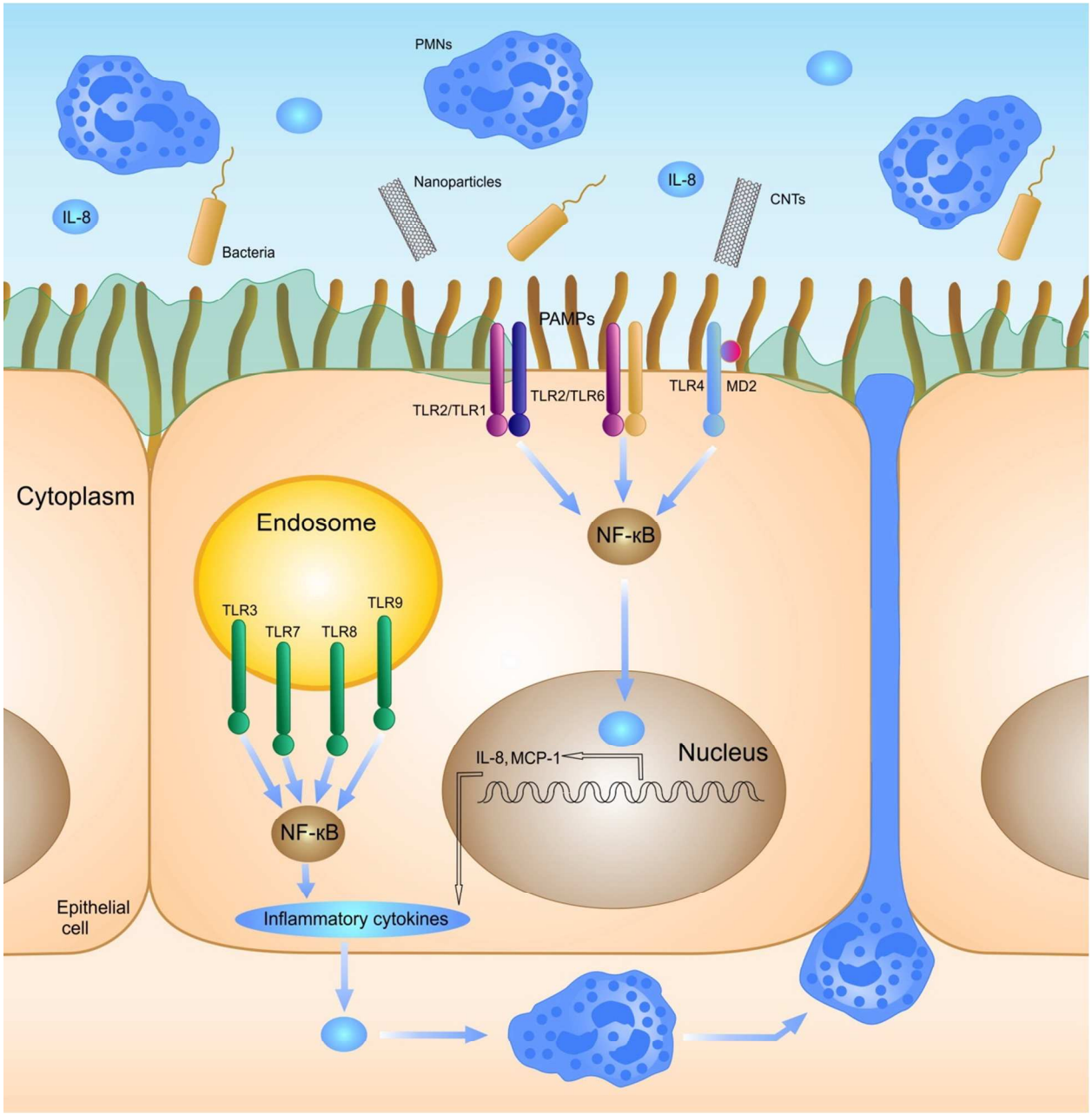

Figure 1. Front and top views of the Sitemap calculated hydrophobic areas (solid yellow surfaces) for TLR1/TLR2 (a,b), TLR2/TLR6 (c,d), TLR4/MD-2 (e,f), TLR2 (g) and TLR5 heterodimer (h).

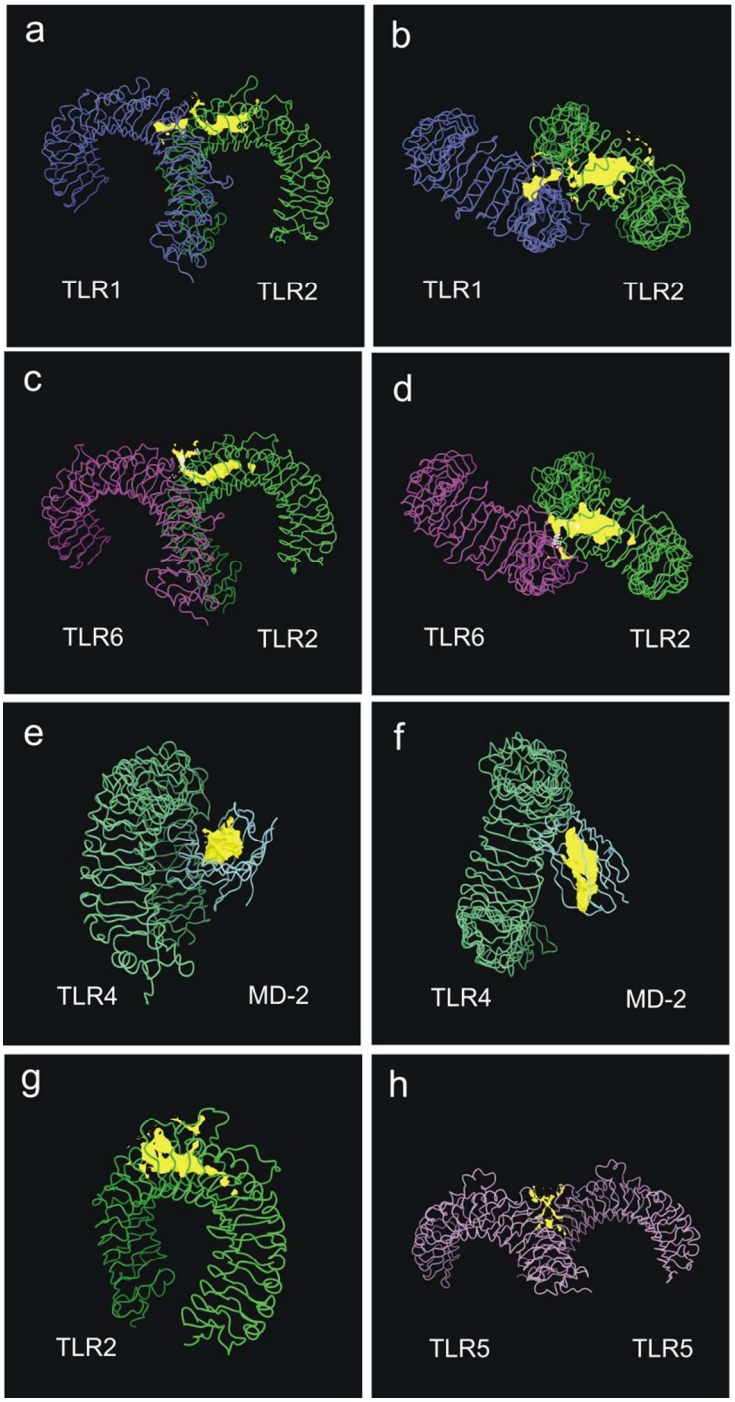

Figure 2. 5,5 CNT-bound TLR1/TLR2 ECDs: **a.** 5,5, CNT is bound to the TLR1 and TLR2 ECDs interface dimerization area; **b.** Aligned structures of TLR2 ECDs before (green carbon atoms) and after (blue carbon atoms) Impact OPLS2005 refinement upon binding 5,5, CNT. The orientation of two parallel entrance loops and the side chains of hydrophobic Phe349, Phe325 and Leu328 preventing nanotube from intrusion are shown to be optimized.

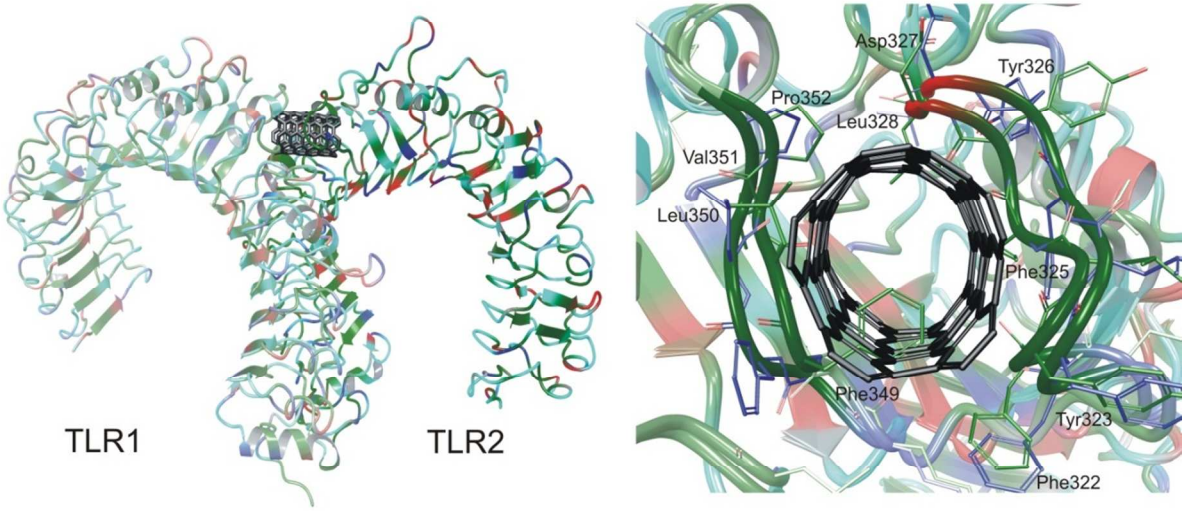

Figure 3. Nanostructures bound TLR4/MD-2 ECD: a. C_{60} is shown to bind inner MD-2 hydrophobic pocket in TLR4/MD-2; Fullerene and carbon nanotube are both well-accommodated in the MD-2 with induced minimal distortion of the entrance residues.